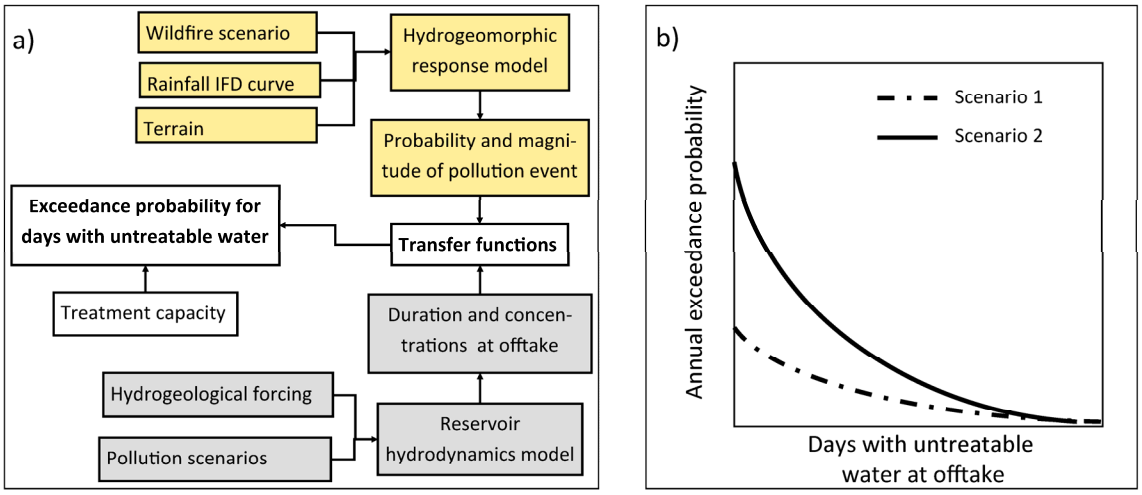

Fig. 1. (a) Model overview showing the workflow for producing a risk metric from transfer functions that couple an erosion model with a reservoir hydrodynamics and reservoir sediment transport model. (b) Example of the final risk metrics which is the probability of consequence. The probability of a range of sediment input events was calculated using a debris-flow response model coupled with storm cells with known AEP from a radar archive. The propagation of sediment from input locations to the reservoir offtake was then modelled using a range of the possible sediment input scenarios.

3.2. Debris-flow response model

The probability of initiating a post-fire debris flow depends on catchment attributes, fire severity and local rainfall regime. The model of post-fire debris flow-initiation is described in detail by Langhans et al. (2016). The slope must be steep enough, with sufficient available sediment on the hillslopes, and the soils must be sufficiently impermeable. Debris flow probability model input parameters are derived only from the zero-order convergent basins (~ 2 ha) of each headwater catchment, as these are the potential debris-flow initiation areas (Cannon et al., 2001). The critical rainfall intensity required to initiate a debris flow in each headwater depends on fixed properties such as slope, and other properties that depend on soil and fire severity, which vary in space and time. The probability of initiating a debris flow depends on the probability of receiving a rainfall event that exceeds critical 12-minute rainfall intensity thresholds (I_{12}) in each zero-order basin. Storm cells obtained from an archive of radar rain fields were simulated at random locations within the catchment. The probability of each rainfall event is based on the intensity-frequency-duration (IFD) rainfall statistics for the headwater location provided by the Bureau of Meteorology (BOM).

The magnitude (load in Mg) of a debris flow once it is initiated depends principally on the slope of the catchment and on the amount of runoff and sediment available for erosion, which is often strongly related to the catchment area. Here we predict the volume of the debris flow (once initiated) using a slope-area landscape analysis described in Nyman et al. (2015). Volumes of debris flow were calculated for each headwater individually at the outlet of first-order streams. The models estimate debris-flows volumes based on characteristics of only the zero- and first-order basins with the outlets located at the point where second-order streams begin. Scour or deposition of sediments in channels between the outlet of first-order streams and the reservoir are neglected. During implementation of the model with simulated storms, all the loads from first-order catchments were accumulated for cases where rainfall intensities exceeded debris-flow thresholds.

The particle size distribution of sediment delivered by debris flows (Table 1) were calculated from size distribution data collected from hillslopes, colluvium, and channels where post-fire debris flows have occurred in the past (Nyman, 2013). For particles with diameter (D) < 1 mm, the distribution was obtained with a laser particle size analyzer. For $D \geq 1$ mm, the distribution was obtained by sieving (30 mm > $D \geq 1$) and visual assessment ($D \geq 30$ mm). When calculating the particle size distribution at the outlet of headwaters, the particle size distribution was summed by weighting the source distributions (hillslopes vs colluvium) by their relative contribution to the total volume.

Table 1. Particle size of debris-flow material from (Nyman, 2013)

Particles	Size range [mm]	Proportion [%]
>Sand	$D>2$	62
Sand	$2> D \geq 0.02$	16
Silt	$0.02>D\geq0.002$	14
Clay	$D<0.002$	8

3.3. Propagation of pollutant plumes within the reservoir

The three-dimensional Aquatic Ecosystem Model (AEM3D) is a coupled hydrodynamics and water quality (including sediments) model that was used to simulate the propagation of the sediment plume through the Upper Yarra reservoir. AEM3D is built on a finite volume numerical grid scheme (Hodges et al., 2000) that solves the unsteady, viscous Navier-Stokes equations for incompressible flow. The model was forced using meteorological data collected from a weather station moored near the dam wall and inflow and outflow monitored by the Melbourne Water Supervisory Control and Data Acquisition (SCADA) system. Thermistor chain data from the same mooring and boat deployed conductivity-, temperature- and depth- (CTD) profiles have been used in previous studies to calibrate the model. The post-fire debris-flow sediment loads (in Mg) were input into the model at four locations around the perimeter of the reservoir that have high probabilities of generating debris flows after fire. Particle densities used in the model are rock/gravel = 2.22 g cm^{-3} and primary soil particles (D < 0.02 mm) = 2.65 g cm^{-3}. The number of days with untreatable water at the water offtake was calculated assuming a sediment concentration threshold of 5 mg L^{-1}.

4. Results

4.1. Debris-flow response model

Rainfall thresholds for post-fire debris flows (I_{12}) range from ~50 to >250 mm h^{-1} (Fig 2a). The headwaters with lower rainfall thresholds are located near the reservoir at lower elevations where the mean annual precipitation is lower and where infiltration rates are lower. The rainfall thresholds in the upper region of the catchment are very high (> 250 mm h^{-1}), and therefore highly unlikely to produce debris flows. Annual exceedance probabilities (AEPs) range from ~ 0.5 for I_{12} = 50 mm h^{-1} to < 0.01 for I_{12} > 250 mm h^{-1}. The modelled clay loads from individual headwaters ranged from 5.5 to 398 Mg with a median of 62 Mg (Fig 2b).

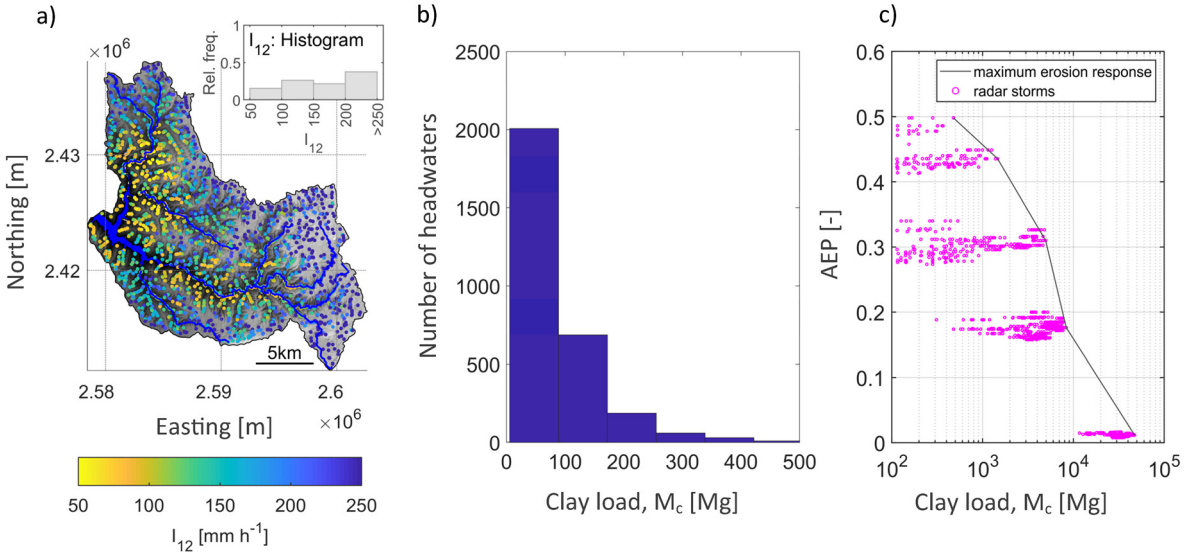

Fig. 2. (a) Rainfall thresholds for post-fire debris flows in the Upper Yarra catchment (b) Distribution of clay loads, M_c, expected from individual first-order headwaters in the case of a debris flow. (c) Annual exceedance probability (AEP) of clay loads inputs to reservoir from debris flows after high-severity fire.

When simulating debris-flow response, the spatial variation in I_{12} means that the probability distribution of clay loads is very sensitive to where storms are located. The distributions of AEPs are shown for locations that are centered on cells in a 10 x 10 grid (grid cells = 3 x 3 km) over the catchment area (Fig 2c). The mass of clay, M_c, from debris flows entering the reservoir for a given storm varies depending on where the storm is located. For an AEP of ~0.3 the M_c ranges from 100 Mg to 5000 Mg depending on where the storm is located. The magnitude of spatial variation in probabilities decrease with the AEP of the rainstorm.

4.2. Propagation of pollutant plumes within the reservoir

The propagation of clay-sized particles to the reservoir offtake was not very sensitive to where sediment was input to the reservoir (Fig 3). For sediment classes greater than clay-sized, deposition on the reservoir bed occurred before they reached the offtake. Within clay-sized particles, it is the very fine fraction (D < 0.001 mm) that contribute to suspended sediment concentration at the offtake. Thus, the impact of an erosion event on concentration at the offtake is highly sensitive to the particle size distribution of the sediment delivered to the reservoir. The number of days exceeding a treatment threshold depends on the clay load, with clay loads of about 8000 Mg causing between 450 to 550 days exceeding 5 mg L^{-1} and clay loads of about 1000 Mg causing about 75 to 100 days exceeding 5 mg L^{-1}. The relation is non-linear with the duration of exceedance increasing at a slower rate when at high input loads (Fig 3).

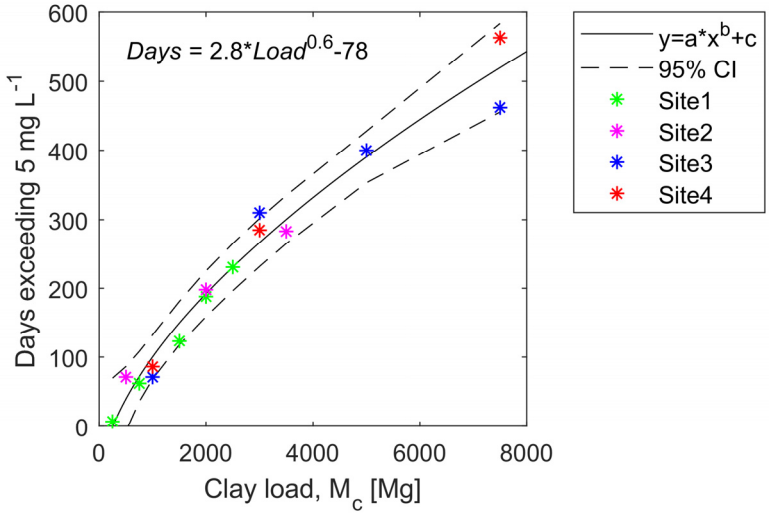

Fig. 3. The relation between days of suspended sediment exceeding 5mg L^{-1} and input of clay at different sites (1-4) around the Upper Yarra reservoir.

4.3. Probability of consequence

Combining the results in Fig 2c and Fig 3 gives a distribution of probabilities for days of interrupted supply (Fig 4). The distributions are different depending on where in the catchment the storm cells are centered. However, all distributions are equally likely. Thus, the maximum impact shown in solid black line in Fig 4 is the most relevant one because that represents the highest risk to reservoir water quality. The duration of undeliverable water for exceedance probabilities of 0.5, 0.4, 0.3, 0.2 and 0.1, marked with arrows in Fig 4, are 15, 130, 320 and 450 and 900 days, respectively. When centered on an erosion hotspot, a storm with an AEP of ~0.3 will produce about 2000 Mg of clay from debris flows. This equates to ~30 times the median clay load (i.e. 62 Mg) from debris-flow producing headwaters.

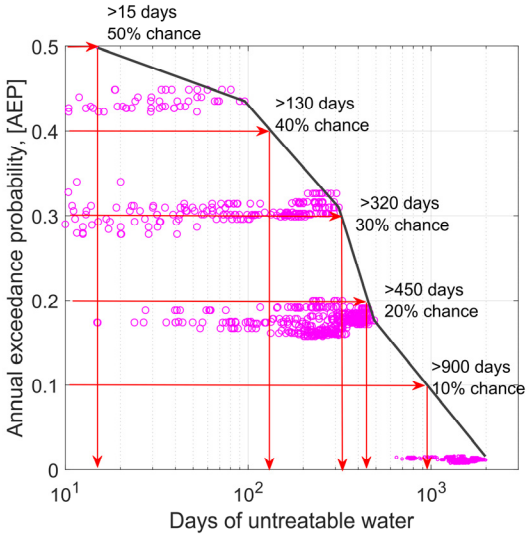

Fig. 4. Annual exceedance probabilities (AEPs) for days of undeliverable water. Based on results in Fig 2c and Fig 3. The scatter plot is the number of days that water exceeds treatability threshold for storms cells with different exceedance probabilities. The variation stems from storm cells being centered on different locations in the catchment. The solid black line is the AEP when storms are centered at a location most susceptible to debris flows.

5. Discussion

Using a novel method for quantifying water quality risk we estimate that a high severity wildfire in the Upper Yarra catchment can lead to water supply interruptions lasting for periods of months to years. The debris-flow susceptibility is spatially variable within the catchment, with hotspots on the eastern flank of the northern reservoir arm representing highest risk. These areas receive lower annual rainfall and have soil properties that are more likely to produce runoff than the those in high rainfall areas at higher elevation. This pattern stems from the way in which infiltration is parametrized in the debris-flow response model, where aridity and fire severity are both causing variation in infiltration (Langhans et al., 2016; Van der Sant et al., 2018).

Much of the risk in Upper Yarra catchment can be attributed to a very small area. Thus, mitigation efforts can be highly targeted at specific areas of the water supply catchment. Possible means for risk mitigation could be fuel reduction burning in these areas to reduce fire intensity in the event of a wildfire. Post-wildfire hillslope treatments such as mulching or small check dams may also be possible mitigation options, to reduce loads and increase debris-flow thresholds. In other water supply catchments, such as the Thomson Reservoir further to the east, the area of dry forest is much larger, and it is likely that the risk will be distributed more broadly.

Future work will include using different fire severity distributions in the model to evaluate the how risk can be mitigated with fuel treatment. By modifying fire severity, it is possible to determine the cost and benefits of carrying out planned (or controlled) burning within the catchment. Model outputs are very sensitive to how storms are modelled, and future work may focus on other methods to model storms. In this paper we have used rain fields from radar to simulate possible erosion scenarios given storms with different return intervals. Using design storms and depth area reduction factors to simulate storms is another way of representing storms. Other approaches are available. There may be opportunities for instance to simulate designs storms using a 2D stochastic rainfall generators (e.g. Peleg et al., 2017). In future modelling efforts, the uncertainty stemming from rainfall, fire severity distributions and the two major model components will be quantified to give some error bounds on the predictions in Fig 4.

The model was developed using the Upper Yarra catchment (and reservoir) as a case study. However, the approach of linking reservoir hydrodynamics with an event-based erosion model to quantify risk is generally applicable and could be applied to debris-flow prone water supply catchments elsewhere. The approach can be easily adapted to operate with debris-flow models that have been developed for other hydro-geomorphic settings (e.g. Gartner et al., 2014).

Acknowledgements

The work is funded by ARC Linkage grant LP150100654, Melbourne Water Corporation and the Victorian Department of Environment, Land, Water and Planning (DELWP).

References

Aven, T., 2011, On some recent definitions and analysis frameworks for risk, vulnerability, and resilience: Risk Analysis, v. 31, no. 4, p. 515-522, doi:10.1111/j.1539-6924.2010.01528.x.

Bladon, K. D., Emelko, M. B., Silins, U., and Stone, M., 2014, Wildfire and the Future of Water Supply: Environmental Science & Technology, v. 48, no. 16, p. 8936-8943, doi:10.1021/es500130g.

Cannon, S. H., Kirkham, R. M., and Parise, M., 2001, Wildfire-related debris-flow initiation processes, Storm King Mountain, Colorado: Geomorphology, v. 39, no. 3-4, p. 171-188, doi:10.1016/S0169-555X(00)00108-2.

Dowdy, A. J., 2017, Climatological Variability of Fire Weather in Australia: Journal of Applied Meteorology and Climatology, v. 57, no. 2, p. 221-234, 10.1175/JAMC-D-17-0167.1

Gartner, J. E., Cannon, S. H., and Santi, P. M., 2014, Empirical models for predicting volumes of sediment deposited by debris flows and sediment-laden floods in the transverse ranges of southern California: Engineering Geology, v. 176, p. 45-56, doi: 10.1016/j.enggeo.2014.04.008.

Guerreiro, S. B., Fowler, H. J., Barbero, R., Westra, S., Lenderink, G., Blenkinsop, S., Lewis, E., and Li, X.-F., 2018, Detection of continental-scale intensification of hourly rainfall extremes: Nature Climate Change, doi:10.1038/s41558-018-0245-3.

Hodges, B., Imberger, J., Saggio, A., and Winters, K. B., 2000, Modeling basin-scale internal waves in a stratified lake: Limnology And Oceanography, v. 45, no. 7, p. 1603-1620, doi: 10.4319/lo.2000.45.7.1603.

Hosseini, M., Nunes, J. P., Pelayo, O. G., Keizer, J. J., Ritsema, C., and Geissen, V., 2018, Developing generalized parameters for post-fire erosion risk assessment using the revised Morgan-Morgan-Finney model: A test for north-central Portuguese pine stands: CATENA, v. 165, p. 358-368, doi:10.1016/j.catena.2018.02.019.

Langhans, C., Smith, H. G., Chong, D. M. O., Nyman, P., Lane, P. N. J., and Sheridan, G. J., 2016, A model for assessing water quality risk in catchments prone to wildfire: Journal of Hydrology, v. 534, p. 407-426, doi:10.1016/j.jhydrol.2015.12.048.

Martin, D. A., 2016, At the nexus of fire, water and society: Philosophical Transactions of the Royal Society B: Biological Sciences, v. 371, no. 1696, p. 20150172, doi:10.1098/rstb.2015.0172.

Nyman, P., 2013, Post-fire debris flows in southeast Australia: initiation, magnitude and landscape controls [Ph.D. Thesis]: Melbourne University of Melbourne, 214 p.

Nyman, P., Sheridan, G. J., and Lane, P. N., 2013, Hydro-geomorphic response models for burned areas and their applications in land management: Progress in Physical Geography, v. 37, no. 6, p. 787-812, doi:10.1177/0309133313508802.

Nyman, P., Sheridan, G. J., Smith, H. G., and Lane, P. N. J., 2011, Evidence of debris flow occurrence after wildfire in upland catchments of south-east Australia: Geomorphology, v. 125, no. 3, p. 383-401, doi:10.1016/j.geomorph.2010.10.016.

Nyman, P., Smith, H. G., Sherwin, C. B., Langhans, C., Lane, P. N. J., and Sheridan, G. J., 2015, Predicting sediment delivery from debris flows after wildfire: Geomorphology, v. 250, p. 173-186, doi:10.1016/j.geomorph.2015.08.023.

Peleg, N., Fatichi, S., Paschalis, A., Molnar, P., and Burlando, P., 2017, An advanced stochastic weather generator for simulating 2-D high-resolution climate variables: Journal of Advances in Modeling Earth Systems, v. 9, no. 3, p. 1595-1627, doi:10.1002/2016MS000854.

Riley, K. L., Bendick, R., Hyde, K. D., and Gabet, E. J., 2013, Frequency–magnitude distribution of debris flows compiled from global data, and comparison with post-fire debris flows in the western U.S: Geomorphology, v. 191, no. 0, p. 118-128, doi: 10.1016/j.geomorph.2013.03.008.

Sheridan, G., Lane, P., Smith, H., and Nyman, P., 2009, A rapid risk assessment procedure for post-fire hydrologic hazards: 2009/10 fire season: Technichal Report for the Victorian Department of Sustainability and Environment, Melbourne, Australia, ISBN 9780734041470, 20 p.

Smith, H. G., Sheridan, G. J., Lane, P. N. J., Nyman, P., and Haydon, S., 2011, Wildfire effects on water quality in forest catchments: A review with implications for water supply: Journal of Hydrology, v. 396, no. 1-2, p. 170-192, doi:0.1016/j.jhydrol.2010.10.043.

Staley, D. M., Negri, J. A., Kean, J. W., Laber, J. L., Tillery, A. C., and Youberg, A. M., 2016, Prediction of spatially explicit rainfall intensity-duration thresholds for post-fire debris-flow generation in the western United States: Geomorphology, v. 278, p. 149-162, doi: 10.1016/j.geomorph.2016.10.019.

Van der Sant, R., Nyman, P., Noske, P., Langhans, C., Lane, P., and Sheridan, G., 2018, Quantifying relations between surface runoff and aridity after wildfire: Earth Surface Processes and Landforms, doi:10.1002/esp.4370.

Westerling, A. L., Hidalgo, H. G., Cayan, D. R., and Swetnam, T. W., 2006, Warming and earlier spring increase western US forest wildfire activity: Science, v. 313, no. 5789, p. 940-943, doi: 10.1126/science.1128834.

White, I., Wade, A., Worthy, M., Mueller, N., Daniell, T., and Wasson, R., 2006, The vulnerability of water supply catchments to bushfires: Impacts of the January 2003 wildfires on the Australian Capital Territory: Australian journal of water resources v. 10, no. 2, p. 1-16, doi: 10.1080/13241583.2006.11465291.